Combustion and Flame 227 (2021) 95–105

Contents lists available at ScienceDirect

Combustion and Flame

journal homepage: www.elsevier.com/locate/combustflame

Exploring the chemical kinetics on oxygen addition reactions of o-xylyl radical at the low temperature

Lili Ye[a], Dezhi Wang[b], Huiting Bian[c,*], Bei Li[a], Wei Gao[a], Mingshu Bi[a]

[a] School of Chemical Engineering, Dalian University of Technology, Dalian 116024, China
[b] PetroChina Coalbed Methane Company Limited, Beijing 100028, China
[c] School of Mechanics and Engineering Science, Zhengzhou University, Zhengzhou, Henan 450001, China

ARTICLE INFO

Article history:
Received 20 August 2020
Revised 29 December 2020
Accepted 2 January 2021
Available online 14 January 2021

Keywords:
o-xylene
Low temperature oxidation
First oxygen addition
Second oxygen addition
Reaction kinetics

ABSTRACT

o-Xylene oxidation displays an autoignition behavior similar to alkanes at low temperatures. This paper presents a detailed investigation of the chemical kinetics of oxygen additions with the *o*-xylyl radical that control the ignition reactivity of *o*-xylene at low temperatures. High-level electronic structure calculations, transition state theory, and master equation simulations are combined to predict the rate coefficients of main elementary reactions. For the initially formed *o*-methylbenzylperoxy (ROO) in the first oxygen addition *o*-xylyl + O_2, its isomerization to *o*-hydroperoxymethyl-benzyl (QOOH) proceeds with a much smaller branching ratio compared to the counterpart ROO → QOOH in alkanes. Despite the slow formation of QOOH, the absence of fast dissociation pathways enable QOOH concentration to build up. QOOH that has the unpaired electron located on a side-chain carbon can readily react with a second molecular oxygen. The QOOH + O_2 reaction then efficiently leads to the growth of the radical pool through a highly chain-branching reaction sequence QOOH + O2 → 2-hydroperoxymethylbenzaldehyde + OH → 1,2-diformylbenzene + 2OH + H. The predicted oxygen addition kinetics offers a good explanation for the alkane-like autoignition behavior of *o*-xylene. Meanwhile, as the key intermediate to chain branching, the lower yield of QOOH results in its lower ignition reactivity. The present study shows that classical low temperature scheme is also valid for benzylic-type hydrogens and radicals of *o*-xylene where the transferred hydrogen from the *ortho*-methyl chain facilitates the isomerization ROO ↔ QOOH. It is also easy to deduce that for *m*- and *p*-xylenes, where no such isomerization step is available, little reactivity should be expected at the low temperature.

1. Introduction

Aromatic hydrocarbons are important components of liquid transportation fuels [1]. The concentration of this subset usually ranges within 20–31% in gasoline, 15–40% in diesel, and 8–25% in jet fuels [2–4]. As opposed to alkanes and cycloalkanes, the presence of benzene ring in aromatics leads to a lower reactivity in chemical reactions on one hand and a higher sooting tendency on the other. Also, aromatic hydrocarbons have the capacity to enhance the anti-knocking property of transportation fuels while mixed in the blend. Aimed at comprehensively emulating the combustion properties of practical fuels in real engines, such as ignition and extinction, flame propagation and pollutant formation, recent surrogate kinetic models often contain aromatic hydrocarbons with a significant fraction in the multi-fuel mixture, which consists of a limited number of constituents and better models combustion systems than the single-fuel mechanisms [5]. This suggests, the predictability of multi-fuel chemical kinetic mechanism depends on the accuracy of the kinetic mechanism of each individual component in the surrogate mixtures.

Xylenes, the smallest multi-substituted aromatic hydrocarbon, have a relatively high concentration in commercial fuels [6]. Compared with toluene, xylenes match better with the real fuel in terms of a larger molecular weight and a more complex structure, and therefore have been proposed as representatives of the family of aromatic species in surrogate mixtures [7–9]. The growth in the molecular size of xylenes leads to an increase in the complexity of the chemical reactions, the most important of which are found to happen at low combustion temperatures [10,11]. Albeit complex, these reactions are very interesting especially in consideration of the effect induced by the isomers and deserve an in-depth characterization of the energetics and kinetics. Unlike the enormous quantity of investigations on toluene, detailed kinetic mechanisms for xylenes are extremely scarce and reports are even rarely

* Corresponding author.
E-mail addresses: bianht@zzu.edu.cn (H. Bian), libei422@dlut.edu.cn (B. Li).

https://doi.org/10.1016/j.combustflame.2021.01.002
0010-2180/

encountered at the low temperatures. As important candidates for surrogate fuels, there is clearly a demand for xylenes to have a established chemical kinetic mechanism.

The low temperature oxidation is the primary mechanism that controls the ignition behaviors [12], and its chemical kinetics is closely related to the practical engine problems like octane numbers and engine knocking [13]. The low temperature combustion also lies at the core of novel engine technologies such as homogeneous charge compression ignition (HCCI) and premixed charge compression ignition (PCCI), where the gas mixture is highly compressed and ignited. The classical low temperature scheme, which explains the prominent reactivity of alkanes at temperatures below 900 K, is characterized with sequential oxygen addition processes [14]. Fundamental kinetic studies have revealed that the addition of molecular oxygen to fuel radicals leads to low temperature chain branching only when the transfer of hydrogen occurs easily in the isomerization steps [12,15]. As for aromatics, when easily transferred hydrogen atoms is available for selective radicals like peroxy radicals, the classical low temperature scheme is also valid to allow for chain branching and leads to a low temperature reactivity. Otherwise, branching occurs via completely different pathways and requires higher temperature.

The existence of two methyl chains gives rise to three xylene isomers, i.e., *o*-xylene, *m*-xylene and *p*-xylene. Early in 2000, Roubaud et al. [16] studied the auto-ignition features of eleven alkylbenzenes including xylene isomers in 600–900 K in a rapid compression machine. In the experiment, *o*-xylene was observed to exhibit a two-stage ignition and negative temperature dependence of ignition delays, with 1,2,3-trimethylbenzene, 1,2,4-trimethylbenzene, 2-ethyltoluene and *n*-propylbenzene also belonging to the same group that showed a complex behavior similar to alkanes. Rather, *m*-xylene and *p*-xylene, together with toluene and 1,3,5-trimethylbenzene, belonged to the other group that could not be ignited below 900 K and 16 bar. Chemical analyses have elucidated that the higher reactivity of the *o*-xylene group (i.e., former group) could be attributed to the close proximity or length of the alkyl chains. Specific for the xylene isomers, *o*-xylene, in which the two methyl carbon atoms are linked together in *ortho*-position on the benzene ring, has a higher degree of reactivity than *m*-xylene and *p*-xylene with the two methyl carbon atoms in *meta*- and *para*-positions.

Limited available oxidation studies of xylenes at low temperatures either centered on the measurement of combustion characteristics, such as ignition delay times [16,17], laminar flame speed and extinction stretch rates [11,18,19], or on identification of species generated during the experiment [20-23]. The ignition delay times were measured either in the rapid compress machine at 600~900 K by Roubaud et al.[16,17]. or in a shock tube at 941~1408 K by Shen et al. [24]. These studies all agreed that *o*-xylene is the most reactive of the three isomers, and Shen et al. concluded that *p*-xylene are almost identical to measurements for toluene at the same conditions. Identification of species were usually performed by probing product samples using on-line equipment such as GC and GC-MC. While the literature reports measurements on oxidation characteristics, few provided concrete chemical kinetic analysis for elementary reaction steps involved. Existing kinetic models that contain xylenes as effective constituents usually refer to analogous reactions of toluene for corresponding rate coefficients. While the mechanism constructed this way is probably of acceptable accuracy for *m*-xylene or *p*-xylene, it is prone to significant uncertainties for *o*-xylene due to the enhanced reactivity by the two adjacent methyl chains. da Silva et al. [25] studied how the ignition reactivity of methylbenzenes is controlled by the number and position of methyl groups. The authors provided quantum chemical calculations for several important reaction steps in the oxidation of *o*-xylyl radical by using the G3SX(MP3) method, providing a preliminary explanation of the autoignition chemistry of *o*-xylene. However, no predictions were made for the rate coefficients in their study. *o*-Xylyl is the most important and most abundant initial radical of *o*-xylene combustion, formed via abstraction or dissociation of the weak methyl H atoms. The present work aims to provide an exhaustive exploration into the detailed chemical kinetics of the first and second oxygen addition reactions of *o*-xylyl at low temperatures. These efforts contribute to probing the underlying mechanism of the *ortho*-effect in enhancing ignition reactivity and are expected to enrich the kinetic database of aromatics and to facilitate the development of surrogate models as a good starting point.

2. Methods

2.1. Electronic structure methods

In current reaction systems, the two radicals that react with oxygen molecule are *o*-xylyl and *o*-hydroperoxymethyl-benzyl (ref. Fig. 1). Note that the latter is the only important QOOH radical generated in *o*-xylyl + O_2. The reaction of *o*-xylyl with molecular oxygen encompasses various types of elementary reactions including addition, isomerization, decomposition, and hydrogen abstraction [14]. For reliability of the theoretical calculations, the compound model chemistries of G4 and CBS-QB3 are employed to compute the energetics and ro-vibrational properties of stationary points on the potential energy surfaces.

At the G4 level of theory, the optimized geometries and vibrational frequencies are obtained at the B3LYP/6–31G(2df,p) level, followed by HF energy limit and a sequence of single point correlation energy corrections using CCSD(T), MP4 and MP2 methods [26]. The G4 theory is assessed to have a significant improvement over the G3 theory, with the improvement largely coming from the inclusion of the HF limit energy. At the CBS-QB3 level of theory, the optimized geometries and vibrational frequencies are obtained at B3LYP/6–311G(2d,d,p), also followed by a variety of single point energy corrections [27]. The CBS-QB3 method makes a good compromise between computational cost and achievable accuracy and is frequently used for reaction systems with more than seven heavy atoms. For the entrance channels of *o*-xylyl + O_2 and QOOH + O_2, the interaction potentials at the transition state region along the reaction coordinate are calculated to determine the variational effect.

The transition states are verified to connect the correct reactants and products by performing the intrinsic reaction coordinate (IRC) analysis [28]. Notably, a fully optimized structure with one imaginary frequency corresponding to the reaction coordinate is located for each entrance channel of *o*-xylyl + O_2 and *o*-hydroperoxymethyl-benzyl + O_2, i.e., TS_1st+O_2 and TS_2nd+O_2, respectively in Fig. 1. That can be attributed to the resonant stabilization of *o*-xylyl and *o*-hydroperoxymethyl-benzyl. The two structures resemble the transition states of regular beta-scission reactions, but it will be seen later that they are not the maximum along the reaction coordinates.

For the low frequencies representing torsional rotations, the hindered rotor approximation is applied to compute the density of states, and the B3LYP/ 6–31G(2df,p) level is used to scan the hinderance potential along the specified dihedral angle with an interval of 10°. Gaussian 09 is used to perform the rest of the quantum chemical calculations [29].

2.2. Master equation simulations

The phenomenological rate coefficients of major pathways in *o*-xylyl + O_2 and *o*-hydroperoxymethyl-benzyl + O_2 reactions are

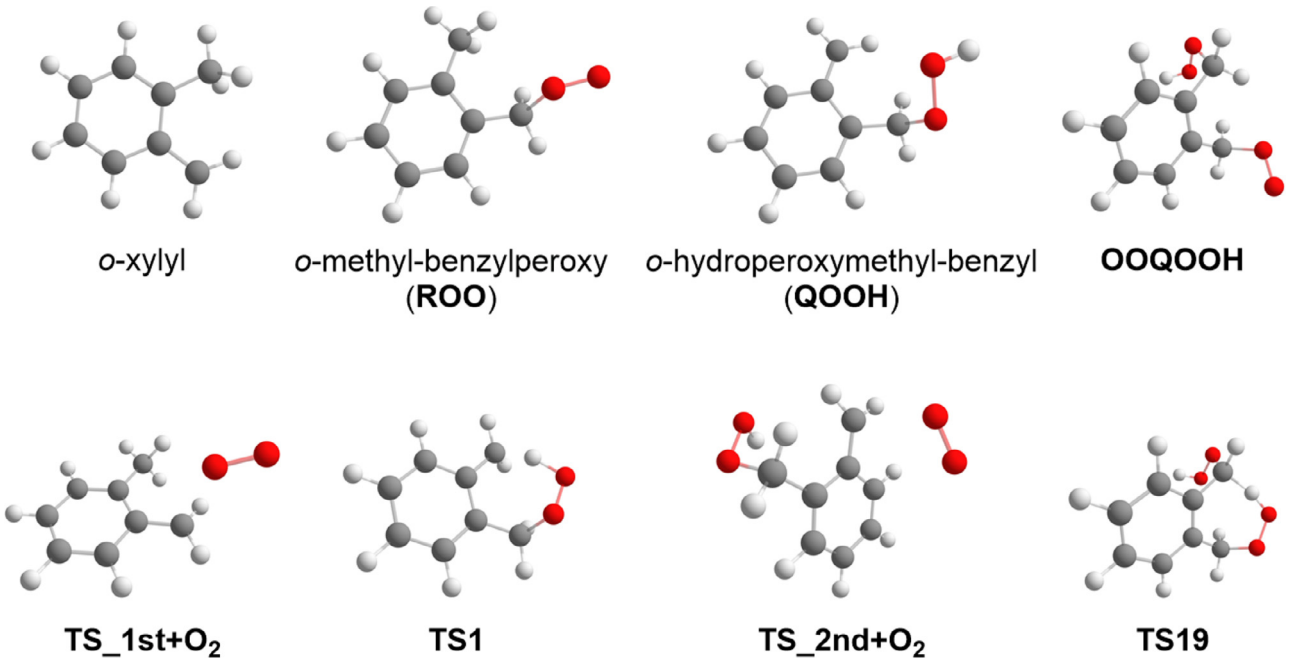

Fig. 1. Structures of key stationary points on potential energy surfaces of oxygen additions with *o*-xylyl.

calculated through solution of the master equation by the Master Equation System Solver (MESS) code [30], covering a temperature range of 400–1700 K and a pressure range of 0.001–1000 atm. The MESS code offers an efficient solution to complex systems that are characterized with multiple interconnected wells and multiple product channels. Eigenvectors and eigenvalues are obtained from solving the master equation, and the determination of rate coefficients relies on a separation of the chemical significant eigenvalues (CSEs) and internal energy relaxation eigenvalues (IEREs). The CSEs are correlated with the chemical transformations between wells and products, and the IEREs describe the collisional energy relaxation within each well. At sufficiently high temperature, the fastest CSEs merge into the IERE continuum. The two species involved then rapidly equilibrate with each other and become chemically indistinguishable. The MESS code then adopts a "species merging" technique to deal with this rapid equilibration. [30]

For the reaction steps, the RRKM theory is applied to predict the microscopic rate coefficients within the rigid-rotor harmonic-oscillator framework except that the low frequencies corresponding to torsional motions are approximated as hindered rotors. The conventional transition state theory is applied to all channels except the entrance channels. For the entrance channels, the interaction potentials change much more gently in the transition state region than those of the other channels that have high energy barriers. The location of the optimal transition state is found to vary significantly with temperature. Hence, a microcanonically variational approach is adopted which leads to energy-dependent transition states and ensures that the transition states selected give the minimum rate coefficients. Specifically, we consider different positions along the minimum energy path for the transition state and calculate rate constants corresponding to each position at various temperatures. The minimum rate constants obtained are what we desire. Moreover, the asymmetric Eckart model is used to quantify the quantum tunneling effect at low temperatures [31].

For the collision steps, the Lennard-Jones potential is used to emulate the intermolecular interaction between the target species and bath gas (i.e. Ar). Here, the binary Lennard-Jones collision parameters (ε/cm^{-1}, σ/Å) is estimated to be (354.8, 6.43) for *o*-xylyl, (408.8, 6.533) for *o*-hydroperoxymethyl-benzyl, and (79.2, 3.47) for Ar estimated by the Joback group contribution method [32]. The single-exponential down model is used to describe the energy transfer of excited molecules. The average energy transferred in a deactivating collision takes the form $\langle \Delta E_{down} \rangle = \alpha_{300}\ (T/300)^n$ with $\alpha_{300} = 424$ cm^{-1}, $n = 0.62$, as recommended by Jasper et al. [33]

3. Results and discussion

In the present study, the energy schemes of G4 and CBS-QB3 are used to compute the potential energy surfaces of the target reaction systems. Before going into details of the computational results, we first take a look at the performance of these two methods in the reactions of O_2 with ethyl, *n*-propyl, and isopropyl. We did not select toluene as our test system only because the CCSD(T)/CBS calculations used as the reference is computationally prohibitive to us (see below).

3.1. Energy test of O_2 addition with small alkyls

Figure 2 shows a number of representative channels that occur on the potential energy surface of $R + O_2$ for several small alkyl radicals such as ethyl, *n*-propyl, and isopropyl. Note that Fig. 2 is only for the purpose of illustration and should not be expected to represent the actual ordering of energies. In this figure, TS(1,n)H ($n = 3, 4, 5$) represents the transition state for (1,n)H-shift intramolecular isomerization. TS_HO_2 denotes the transition state for the concerted elimination reaction of ROO to produce HO_2 and conjugate alkenes. We have tested the accuracy of G4 and CBS-QB3 for the initial binary reactants, ROO, QOOH, as well as main transition states. As the reference, the CCSD(T)/CBS energies are also computed, which are extrapolated from CCSD(T)/cc-pVTZ and CCSD(T)/cc-pVQZ calculations following the procedure of Halkier et al. [34]

$$E_{CBS} = \left[E_X\ X^3 - E_{X-1}(X-1)^3\right] / \left[X^3 - (X-1)^3\right] \quad (E1)$$

where $X = 4$ for the cc-pVQZ basis set. The geometries and vibrational frequencies are optimized at B3LYP/def2-TZVP, and the zero-point vibrational energy are included in the final energies.

Table 1 lists the computed energies of the stationary points using different methods, together with selective literature data. From

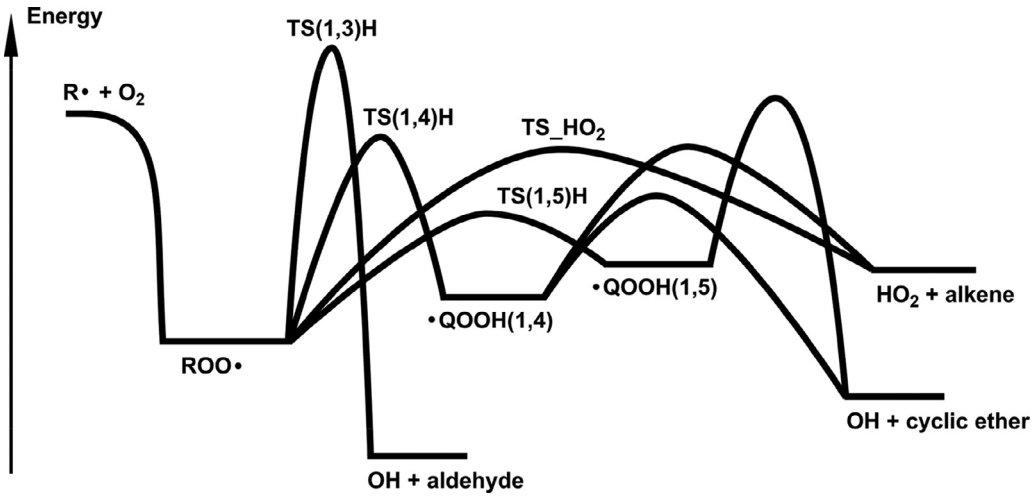

Fig. 2. Schematic plot of classical reaction mechanism of $R + O_2$ for small alkyl radicals. Note that the potential energy diagram is only for an illustration purpose and the ordering of energies does not necessarily represent the actual situation.

Table 1
Zero-point energy corrected energies of key stationary points in reactions of ethyl, *n*-, and iso-propyl with O_2 (at 0 K in kcal/mol).

Key channels in $R + O_2$	CCSD(T)/CBS[a]	G4	CBS-QB3[a]	Miller[b]	Schaefer[c,d], Goldsmith[e]	DeSain[f]
ethyl + O_2						
$CH_3CH_2 + O_2$	0.0	0.0	0.0	0.0	0.0	0.0
CH_3CH_2OO	−33.0	−33.5	−34.1	−33.9[b]	−30.3[c]	−33.5[h]
					−33.0[d]	
CH_2CH_2OOH	−16.4	−16.6	−17.0	−17.0[b]		
TS(1,3)H	9.3	9.8	7.0	8.2[b]		
TS(1,4)H	3.9	3.7	1.8	3.1[b]	5.3[c]	
TS_HO_2	−1.3	−1.7	−2.9	−3.0[b]	−3.0[d]	
***n*-propyl + O_2**						
$CH_3CH_2CH_2 + O_2$	0.0	0.0	0.0		0.0	0.0
$CH_3CH_2CH_2OO$	−33.7	−34.3	−34.9		−33.3[e]	−34.9[g]
						−33.9[j]
$CH_2CH_2CH_2OOH$	−18.3	−18.6	−19.8		−18.1[e]	−19.8[g]
CH_3CHCH_2OOH	−20.7	−20.9	−21.5		−20.4[e]	−21.6[g]
TS(1,3)H	8.4	8.8	6.1			
TS(1,4)H	−0.4	−0.6	−2.8		−0.2[e]	−2.6[g]
						−2.1[h]
						−2.1[j]
TS(1,5)H	−8.7	−8.9	−11.3		−8.5[e]	−11.2[g]
TS_HO_2	−2.0	−3.0	−4.2		−2.7[e]	−5.2[g]
						−3.8[h]
						−3.8[j]
iso-propyl + O_2						
$CH_3CHCH_3 + O_2$	0.0	0.0	0.0		0.0	0.0
CH3CHOOCH3	−34.7	−35.7	−36.2		−34.8[e]	−36.8[g]
						−38.1[i]
						−34.8[j]
$CH_3CHOOHCH_2$	−17.8	−18.5	−18.8		−18.0[e]	−20.2[g]
TS(1,3)H	6.2	6.0	3.4			
TS(1,4)H	1.5	0.8	−0.8		1.2[e]	−1.4[g]
					1.6[k]	−0.2[h]
						0.9[i]
						−1.7[j]
TS_HO_2	−3.5	−4.2	−5.0		−4.2[e]	−7.0[g]
					−3.6[k]	−4.7[h]
						−6.0[i]
						−5.0[i]
						−5.0[j]

[a] B3LYP/def2-TZVP is used for geometry optimization and frequency analysis. Energies at the CBS limit are extrapolated from CCSD(T)/cc-pVTZ and CCSD(T)/cc-pVQZ energies following the Eq. (E1). Literature results by CBS-Q series are not listed.
[b] Miller et al. [35].
[c] The Schaefer refers to the two studies on ethyl + O_2: Rienstra-Kiracofe et al. [36], and Wilke et al. [37].
[d] The Schaefer refers to the two studies on ethyl + O_2: Rienstra-Kiracofe et al. [36], and Wilke et al. [37].
[e] Goldsmith et al. [12].
[f] The DeSain refers to the original PES in ref. 44 and all subsequent modifications:.
[g] DeSain et al. [38].
[h] DeSain et al. [39].
[i] Estupiñán et al. [40].
[j] Huang et al. [41].
[k] Huynh et al. [42].

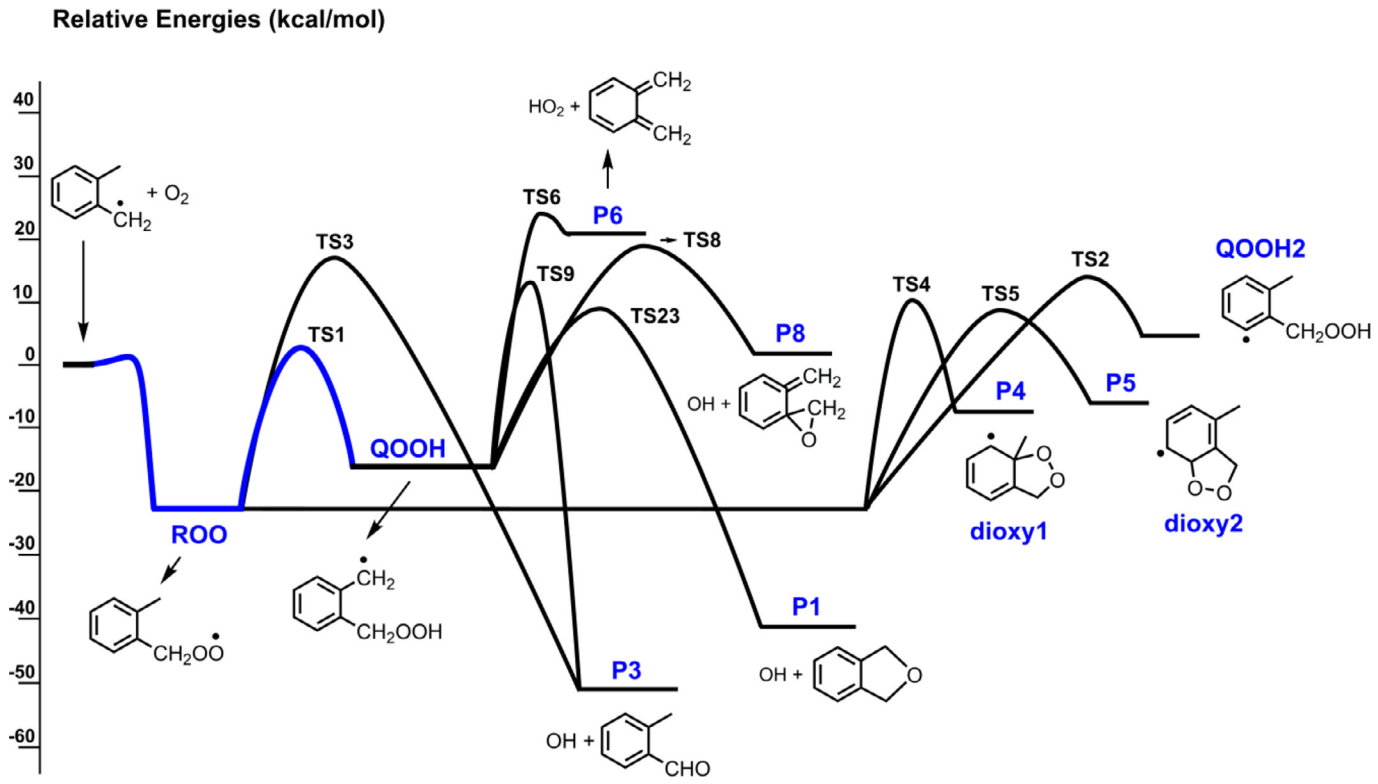

Fig. 3. Relative energies of major reaction pathways on potential energy surface of *o*-xylyl + O_2 at 0 K in kcal/mol. The initial bimolecular reactants are set to be energy zero.

Table 1, G4 energies agree best with the CCSD(T)/CBS results, with the largest discrepancy smaller than 0.5 kcal/mol for ethyl + O_2 and 1.0 kcal/mol for propyl + O_2. CBS-QB3 results lie below both G4 and CCSD(T)/CBS results, and many of the energy discrepancies are larger than 2 kcal/mol. The column DeSain appears to indicate a better agreement with the CBS-QB3 energies, but the subsequent modifications in this column tend to increase the energies. More importantly, the good agreement with the more recent calculations by Goldsmith et al. [12]. shows a better accuracy of G4 and CCSD(T)/CBS results. As a result, the results at G4 theory are recommended.

3.2. Potential energy surface of o-Xylyl + O_2

Figure 3 plots the major reaction routes occurring on the *o*-xylyl + O_2 potential energy surface. The zero-point energy (ZPE) corrected reaction enthalpies and energies under G4 and CBS-QB3 are presented in Table 2. The complete potential energy surface and associated energy values are provided in Fig. S1 of the Supplemental Material.

Like the situation in small alkyl radicals, the CBS-QB3 energies are smaller than the G4 energies for most of the stationary points considered except for ROO, QOOH2, P6 and P8 (the energy deviations are within 0.8 kcal/mol). The energy discordance becomes more significant in the transition states. Compared with literature reports, the G3SX(MP3) results by da Silva et al. [25] reported higher reaction enthalpies for ROO, TS1 and the entrance barrier. The calculations at CASPT2/ANO-L-VDZP//B3LYP/cc-pVDZ by Canneaux et al. [43] are even smaller than CBS-QB3 energies. However, in the current study we still recommend the calculations at G4 out of the high accuracy of this theory. And the lack of literature data implies that, the disagreement between the present study and literature results does not necessarily indicate the inaccuracy of G4.

Table 2
Reaction enthalpies (298 K) and energies (0 K) of key stationary points in *o*-xylyl + O_2 relative to the initial bimolecular reactants (kcal/mol).[a].

Reaction enthalpies (298 K)	G4	CBS-QB3	Literature
***o*-xylyl + O_2**	0.0	0.0	0.0
ROO	−23.7	−23.1	−20.0[c]
QOOH	−16.9	−17.8	
QOOH2	4.2	5.0	
P3	−49.5	−50.2	
P1	−40.9	−42.5	
P8	1.5	2.0	
P6	20.3	21.0	
dioxy1	−9.1	−10.7	
dioxy2	−7.3	−8.8	
entrance barrier[b]	2.2	1.3	2.7[c]
TS_1st+O2	1.0	0.3	
TS1	0.9	−1.0	2.2[c]
TS2	13.2	8.2	
TS3	17.2	15.8	
TS4	8.9	5.8	
TS5	7.6	4.3	
TS6	23.6	19.4	
TS8	19.0	15.9	
TS9	12.4	11.6	
TS23	9.0	6.7	
Reaction energies (0 K)	**G4**	**CBS-QB3**	**Literature**
Δ(TS1 − ROO)	25.5	23.0	22.6[d]
Δ(TS3 − ROO)	41.1	39.1	34.9[d]

[a] For comparison with literature results, the reaction enthalpies (298 K) and reaction energies (0 K) are both presented.
[b] The "entrance barrier" denotes the maximum along the minimum energy path for the entrance channel of *o*-xylyl + O_2.
[c] G3SX(MP3) by da Silva et al. [25].
[d] CASPT2/ANO-L-VDZP//B3LYP/cc-pVDZ by Canneaux et al. [43].

From Fig. 3 and Table 2, the activation energy of initially formed *o*-methylbenzylperoxy radical (ROO) is less than 23.7 kcal/mol. For comparison, the initially formed activated alkylperoxy adducts of alkanes have over 30 kcal/mol excess energy than ground state radicals [12,37,44]. The smaller activation energy of ROO can mainly be ascribed to the resonant stability of the *o*-xylyl radical and largely explains the lower autoignition reactivity than alkyl radicals. For the entrance channel, quantum chemical calculations delineate a flat energy barrier along the minimum energy path. Similar barriers were also found in reaction systems like benzyl + O_2 [25,45]. For instance, da Silva et al. predicted this barrier to be around 2.7 kcal/mol [25].

Forward consumption of ROO proceeds primarily through the intramolecular H-atom transfer reactions. The classical low temperature scheme of alkanes is also valid for *o*-xylyl + O_2, which is rather different from benzyl + O_2. Amongst the three H-shift channels, ROO abstracts the benzylic hydrogen atom from adjacent methyl chain with the lowest barrier and leads to the formation of *o*-hydroperoxymethyl-benzyl through a seven-membered ring transition state TS1. Like the alkane systems, here the *o*-hydroperoxymethyl-benzyl radical is also referred to as QOOH. This radical is going to play a key role in the low-temperature chain-branching of *o*-xylene ignition. The other two H-transfer reactions of ROO include the abstraction of another benzylic hydrogen via a highly strained four-membered ring transition state TS3 and the abstraction of H-atom from the benzene ring via the transition state TS2. Additionally, ROO can isomerize to form two dioxy heterocyclic intermediates through the ring-closure reaction channels P4 and P5. The latter two H-transfer reactions and the ring-closure reactions have a negligible contribution to the ROO decomposition owing to their higher energy barriers. Similarly, the following consumption of QOOH, which produce OH + cyclic oxides/2-methylbenzaldehyde and HO_2 + *o*-xylylene, are noncompetitive in energy when compared with its reverse back to ROO. From the discussion above, the reactions interconnecting *o*-xylyl + O_2, ROO and QOOH in essence dominate the overall kinetics of the *o*-xylyl + O_2 reaction, and the competition between ROO isomerizing to QOOH and ROO dissociating back to reactants is the determining factor for the oxidation reactivity at low temperatures.

On the reaction of *o*-xylyl with molecular oxygen, an H-atom abstraction mechanism is also chemically possible aside from the direct recombination. However, the H-abstraction reaction is uncompetitive at low temperatures owing to the significant activation energy (greater than 30 kcal/mol).

3.3. Kinetics analysis of *o*-xylyl + O_2

As stated in **Methods**, a transition state structure TS_1st+O_2 is located by G4 or CBS-QB3 for the entrance channel of *o*-xylyl + O_2. Since the energy barrier is rather flat, simply placing the dividing surface at TS_1st+O_2 is likely to introduce significant errors in the calculated rate coefficients. Here, a variational approach is implemented to determine the optimal position of the transition state as a function of temperature. Figure 4 presents the interaction potentials in the vicinity of TS_1st+O_2 along the minimum energy path. As seen from the figure, TS_1st+O_2 is not the maximum on the minimum energy path, supporting the implementation of the variational approach. Also shown are the best transition states that minimize the high-pressure limit rate coefficients at different temperatures. As the temperature increases, the transition state shifts to configurations with shorter separation between the two reacting fragments. For instance, in the case of G4 the configuration with a separation of 2.15 Å is the best choice of transition state at 400 K. As the temperature increases to 500 K, the transition state moves to the configuration at 2.10 Å and then to the configuration at 2.05 Å when the temperature rises to 1500 K. In general, the

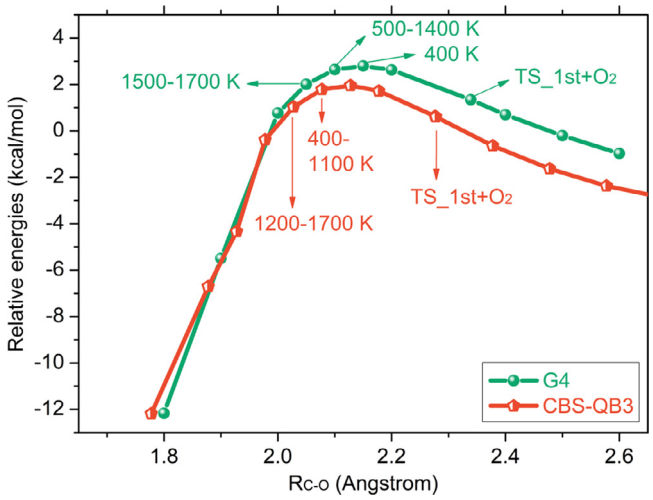

Fig. 4. The interaction potentials in the vicinity of TS_1st+O_2 along the minimum energy path. TS_1st+O_2 is computed via full optimization to have one imaginary frequency that corresponds to the reaction coordinate. The optimal transition states that minimize the rate coefficients at different temperatures are also labeled.

enthalpic and entropic effects combine to result in the position of the transition states, i.e., within the range of 2.05~2.15 Å for G4, and within 2.02~2.07 Å for CBS-QB3.

Figure 5 plots the high-pressure limit rate coefficients of *o*-xylyl + O_2 predicted using G4 and CBS-QB3. At the low temperature end, the predictions via variational minimization are close to calculations using the maximum of interacting potential as the transition state. The divergence at higher temperatures can be attributed to the increasingly important entropic effect in evaluating the sum of states, so the transition state moves toward the adduct side to minimize the rate coefficients. Also, imprudently taking TS_1st+O_2 as the transition state would lead to errors in the rate coefficients by as much as an order of magnitude, as is indicated by the lines with circle and diamond. Figure 5 shows that the G4 predictions are slower than the CBS-QB3 predictions, which is in consistent with the relatively larger energies at G4. To test the effect of energies, we simply increase the energies at CBS-QB3 by 1.5 kcal/mol (the variational calculation). The so obtained rate coefficients, which are represented by the line with star, demonstrate a good agreement with the G4 predictions. Considering the uncertainties of methods, the G4 predictions are conservatively recommended in this study. Since neither measured nor calculated values are found in literature for rate coefficients of *o*-xylyl + O_2, we include in Fig. 5 the rates of phenyl + O_2 and benzyl + O_2 by Zhang et al. [45] In their study, the rate coefficients of benzyl + O_2 are much smaller than those of phenyl + O_2, which can be ascribed to the resonant stabilization of benzyl radical. Our rate coefficients of *o*-xylyl + O_2 at G4 exhibit a sharper increase with temperature but are below the results of benzyl + O_2. The lower entrance barrier in benzyl + O_2 by Zhang et al. [45] probably explains the shallower slope in their study

The temperature-dependent rate coefficients of main channels in *o*-xylyl + O_2 reaction at 1 atm are presented in Fig. 6(a). Here only the calculations using the G4 energetics are displayed. Initial addition to peroxy radical ROO is the only important reaction at low temperatures. Formation to QOOH has the second largest rate constants, followed by the generation of OH + *o*-xylene oxide (P1). The reaction channels leading to OH + 2-methylbenzaldehyde (P3) and to the dioxy heterocyclic intermediates (P4 and P5) are computed to have comparable rate constants. In essence, the formation of products other than ROO can be safely ignored under the conditions investigated. Note that the absence of rate coefficients for the formation of ROO and QOOH at higher temperatures is a

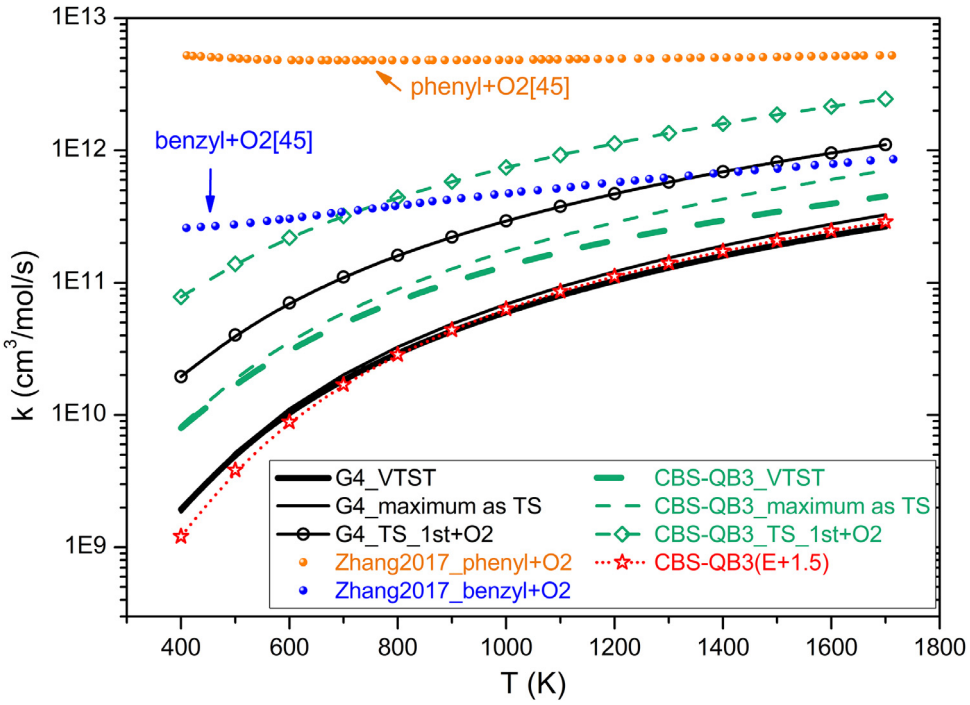

Fig. 5. The high-pressure limit rate coefficients of *o*-xylyl + O_2 recombination using G4 and CBS-QB3 methods. Symbols represent the calculations of phenyl + O_2 and benzyl + O_2 recombination from the work of Zhang et al. [45].

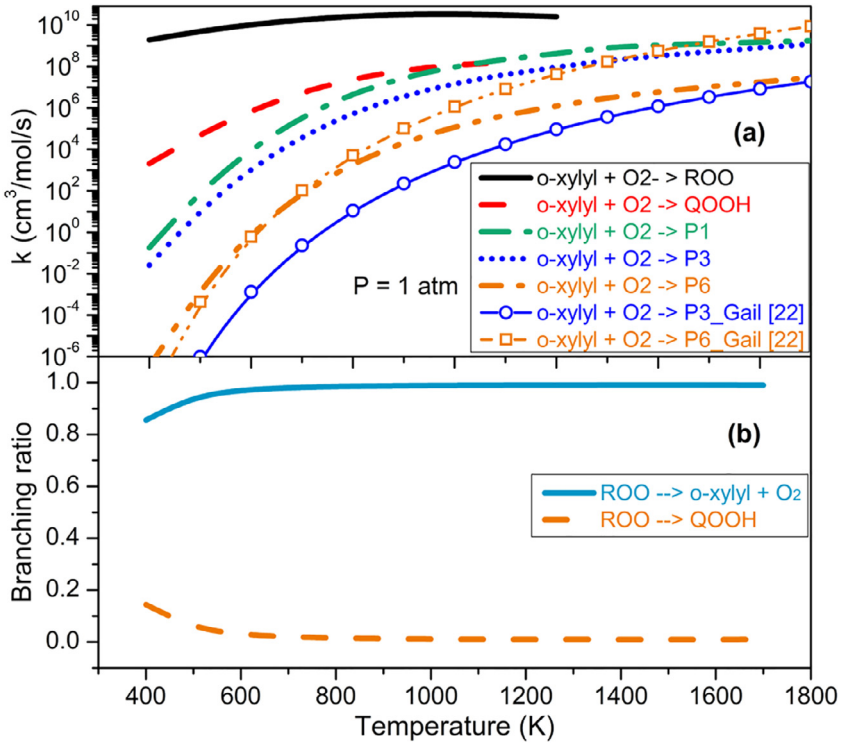

Fig. 6. (a) The temperature-dependent rate coefficients of *o*-xylyl + O_2 recombination at 1 atm and (b) the branching ratio of ROO decomposition channels at high-pressure limit under G4 energetics.

result of the equilibration between ROO and QOOH, which become chemically indistinguishable. Gail et al. [22] in 2008 developed a chemical kinetic model for *o*-xylene to simulate a jet-stirred reactor experiment over 900–1400 K at atmospheric pressure. The rate coefficients of pathways therein are mostly estimated by analogy to similar reactions in *m*- and *p*-xylenes. In Gail's model, the authors provided the rate coefficients of two pathways for *o*-xylyl + O_2, i.e., the product channels of P3 and HO_2 + *o*-xylylene (P6). Here we have also included the calculation results of P3 and P6 in Fig. 6(a) for comparison. The estimations made by Gail et al. are in large discrepancy from the present study, particularly for the channel P3. The authors presumed larger rate coefficients

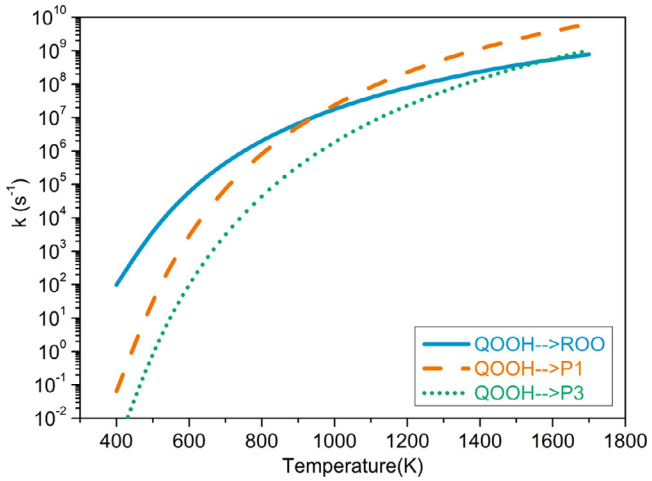

Fig. 7. The temperature-dependent rate coefficients of QOOH decomposition at high-pressure limit.

for the formation of HO_2 + *o*-xylylene (P6) than the formation of OH + 2-methylbenzaldehyde (P3). Whereas in present study, the channel P3 is predicted to be more advantageous in enthalpy and exhibits a more significant quantum tunneling effect. In this sense, the rate coefficients of P3 and P6 estimated by Gail et al. [22] probably have large uncertainties.

Figure 6(a) implies that the following consumption mechanism of ROO should largely dominate the low temperature reactivity of *o*-xylene. Master equation analysis reveals that dissociation back to *o*-xylyl + O_2 and isomerization to QOOH are the two most important channels of ROO consumption. Figure 6(b) plots the branching ratios of these two channels as a function of temperature at the high-pressure limit. Results show that the main fate of ROO is to dissociate back to initial reactants, and isomerization to QOOH plays a role merely below 700 K with the largest branching of 15%. The enhanced rate of isomerization at low temperatures mainly arises from the increased quantum tunneling through the energy barrier TS1. The relatively low yield of QOOH accounts for the lower autoignition reactivity than alkanes where QOOH radicals are formed in abundance from ROO.

Figure 7 compares the rate coefficients of the primary decomposition channels of QOOH. Kinetic predictions demonstrate that the dissociation back to ROO is more preferred than its forward decomposition at temperatures below 900 K. At higher temperatures, the formation of OH + *o*-xylene oxide (P1) is more favored. At low temperatures, the combined effect of rapid equilibration with ROO and slow dissociation channels allows the concentration of QOOH to build up so as to participate in the chain branching chemistry. The formed QOOH is able to react readily with an oxygen molecule and leads to the chain branching process. In the present study, the chemical kinetics of the second oxygen addition (i.e. QOOH + O_2) is also discussed in detail as follows.

The modified Arrhenius parameters for the rate coefficients of major pathways in *o*-xylyl + O_2 reaction are tabulated in Table S1 of the Supplemental Material, which enables direct application in kinetic software like Chemkin.

3.4. Kinetic mechanism of *o*-hydroperoxymethyl-benzyl + O_2

The potential energy surface of the QOOH + O_2 reaction is displayed in Fig. 8, depicted under the G4 energy scheme. The solid lines represent channels of the most importance occurring on this surface, including the initial addition to OOQOOH and its dissociation to the product pair P7. The dissociation barrier, TS19, represents the transfer of benzylic hydrogen from the neighboring side chain, and its lower enthalpy causes an increased flux to the products of P7. The other two decomposition channels of initial adduct, characterized with TS18 and TS21, are not favored due to the relatively high activation energies. The dashed lines illustrate the major decomposition channels of 2-hydroperoxymethyl-benzaldehyde in P7.

Similar to the *o*-xylyl + O_2 reaction, TS_2nd+O_2 with an energy of 0.98 kcal/mol at G4 is not the maximum of the

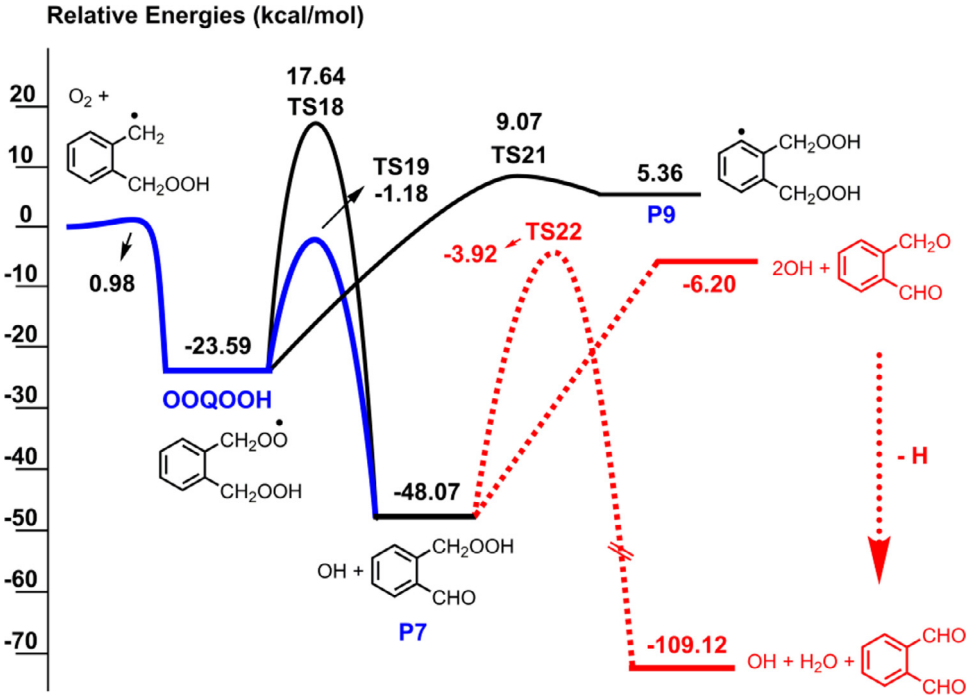

Fig. 8. Potential energy surface of the *o*-hydroperoxymethyl-benzyl + O_2 reaction. The energies are relative to the initial bimolecular reactants at 0 K by G4 in kcal/mol. The dashed lines represent major decomposition routes of 2-hydroperoxymethyl-benzaldehyde of P7.

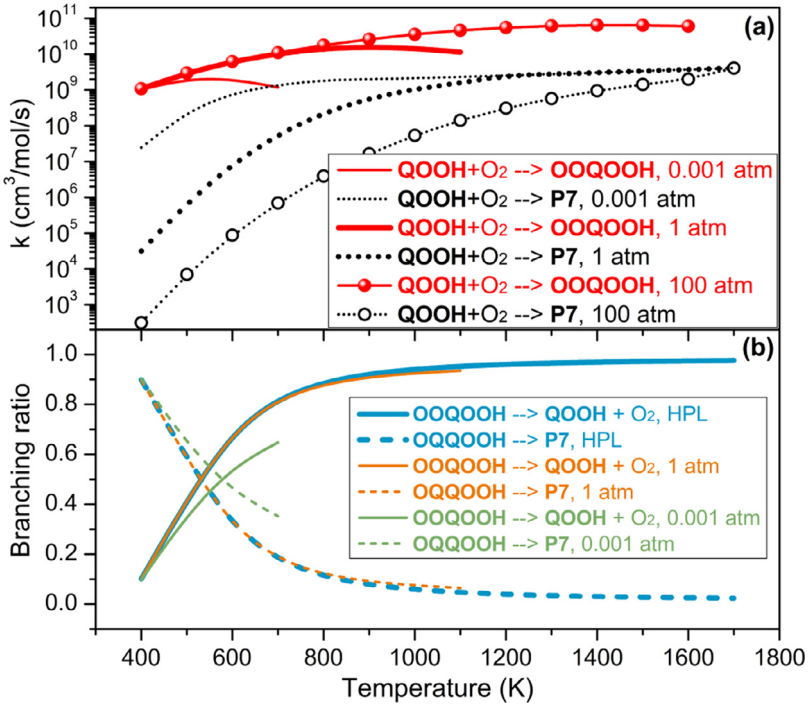

Fig. 9. (a) The temperature-dependent rate coefficients of QOOH + O_2 reaction at selected pressures and (b) the branching ratio of OOQOOH decomposition channels as a function of temperature.

interaction potentials between the reacting moieties. Hence, a variational approach is also applied to minimize the rate coefficients of the entrance channel QOOH + O_2 ↔ OOQOOH. The temperature-dependent rate coefficients of major pathways of QOOH + O_2 at a number of selected pressures are presented in Fig. 9(a). Generally, the initial addition to OOQOOH prevails over the channel P7 under investigated conditions. As the pressure increases, the reaction flux through the former channel gets enhanced while flux through the latter gets reduced. This is because with the pressure increasing a larger portion of the chemically activated adduct is stabilized by collisions into the initial well instead of directly giving rise to P7 through a well-skipping mechanism.

The following-up consumption of OOQOOH, the dominant product of QOOH + O_2, is the key mechanism that affects the accumulation of the radical pool below 900 K and therefore is directly concerned with the low temperature autoignition reactivity. The primary dissociation of OOQOOH mainly includes two channels, that is, the reverse dissociation to initial reactants and the formation of P7 products leading to active OH radical. Figure 9(b) plots the branching ratios of the two channels as a function of temperature at selected pressures. From this plot, the dissociation to P7 product pair makes a larger contribution at the initial stage, but it becomes less important as the temperature goes to medium range. The two channels approximately bisect the overall reaction flux of OOQOOH dissociation at temperature within 530~580 K. The partitioning between the two channels changes with the pressure until about 1 atm above which the pressure has little impact.

Importantly, the benzaldehyde derivative (i.e., 2-hydroperoxymethyl-benzaldehyde in P7) can easily decompose via direct bond fission of the weak O–OH to produce *o*-formylbenzoxyl + OH. The *o*-formylbenzoxyl then loses a hydrogen atom to form 1,2-diformylbenzene. The reaction sequence QOOH + O_2 → P7 → 1,2-diformylbenzene + 2OH + H is a highly chain-branching process and largely explains the alkane-like autoignition behavior of *o*-xylene, which is characterized with a two-stage ignition and the negative temperature coefficient. In summary, the QOOH radical formed in the first oxygen addition, despite in a relatively slow rate, could effectively proceed forward via reacting with a second oxygen molecule and lead to the growth of radical pool. This is expected to greatly enhance the low temperature oxidation reactivity of *o*-xylene. Note that other reactions, such as the recombination of *o*-xylyl with HO_2 radical which converts the inactive HO_2 to active OH, also play a role in the low temperature oxidation. Detailed kinetic analysis of these reactions is on the list of our future work. In addition, at higher temperatures dissociation of *o*-xylyl as well as QOOH takes place before they are collisionally deactivated, and addition of O_2 becomes no longer important.

The modified Arrhenius parameters of major channels in *o*-hydroperoxymethyl-benzyl + O_2 are tabulated in Table S2 of the Supplemental Material.

4. Conclusions

o-Xylene was reported in literature to exhibit a complex, alkane-like, autoignition behavior at low temperature and elevated pressure. The present paper performs a theoretical exploration into the chemical kinetics of the oxygen addition reactions that control the low temperature reactivity via combining quantum chemical calculations and transition state theory based master equation simulations. The first oxygen addition, i.e., the *o*-xylyl + O_2 reaction, gives rise primarily to the initial peroxy adduct, and the decomposition of the peroxy adduct leads to QOOH with a relatively small reaction flux (less than 15% by G4) by transferring a benzylic hydrogen atom from the neighboring methyl group. Although yielded in a small amount, the combined effect of equilibration with peroxy radical and lack of fast dissociation routes allows for QOOH radicals to gradually accumulate. QOOH then reacts readily with a second molecular oxygen via the *o*-hydroperoxymethyl-benzyl + O_2 recombination and leads to the growth of radical concentration through a highly chain-branching reaction sequence. As the key intermediate to chain branching, the limited concentration of QOOH results in the lower reactivity than alkanes for which QOOH radicals are generated in abundance. While at the same

time, it is these limited QOOH intermediates that efficiently promote the low temperature reactivity and account for the alkane-like autoignition pattern of *o*-xylene.

This paper shows that classical low temperature scheme is valid for benzylic-type hydrogens and radicals of *o*-xylene. This can be ascribed to the accessible isomerization step where the transferred hydrogen comes from the *ortho*-methyl chain. Comparing the molecular structures of *o, m*- and *p*-xylenes, it becomes apparent that no such isomerization step happens for the *meta*- and *para*-xylenes due to steric hindrance. This explains why *o*-xylene demonstrates much higher ignition reactivity than its other two isomers. The present study is expected to facilitate the development of multi-fuel chemical kinetic models for practical engine fuels.

Declaration of Competing Interest

The authors declare that they have no known competing financial interests or personal relationships that could have appeared to influence the work reported in this paper.

The authors declare the following financial interests/personal relationships which may be considered as potential competing interests:

Acknowledgments

The authors are grateful to the financial support from National Natural Science Foundation of China (Nos. 51606122, 51906227 and 51904054), Fundamental Research Funds for the Central Universities of China (No. DUT20RC(3)015) and Advanced Innovation Team of Petrochemical Equipment and Safety Systems (No. DUT2020TB03).

Supplementary materials

Supplementary material associated with this article can be found, in the online version, at doi:10.1016/j.combustflame.2021.01.002.

Appendix. Supplementary material

The modified Arrhenius parameters of rate coefficients for important reaction routes in the first and second oxygen additions are provided in the Supplementary Material. Also included are the optimized geometries of stationary points in Figs. 3 and 8.

References

[1] W.J. Pitz, C.J. Mueller, Recent progress in the development of diesel surrogate fuels, Prog. Energy Combust. Sci. 37 (2011) 330–350.
[2] J.T. Farrell, N.P. Cernansky, F.L. Dryer, C.K. Law, D.G. Friend, C.A. Hergart, R.M. McDavid, A.K. Patel, C.J. Mueller, H. Pitsch, Development of an Experimental Database and Kinetic Models For Surrogate Diesel Fuels, 2007.
[3] T. Edwards, M. Colket, N. Cernansky, F. Dryer, F. Egolfopoulos, D. Friend, E. Law, D. Lenhert, P. Lindstedt, H. Pitsch, A. Sarofim, K. Seshadri, M. Smooke, W. Tsang, S. Williams, Development of an Experimental Database and Kinetic Models For Surrogate Jet Fuels, 2007.
[4] W.J. Pitz, N.P. Cernansky, F.L. Dryer, F.N. Egolfopoulos, J.T. Farrell, D.G. Friend, H. Pitsch, Development of an Experimental Database and Chemical Kinetic Models for Surrogate Gasoline Fuels, 2007.
[5] C.K. Westbrook, M. Mehl, W.J. Pitz, G. Kukkadapu, S. Wagnon, K. Zhang, Multi--fuel surrogate chemical kinetic mechanisms for real world applications, PCCP 20 (2018) 10588–10606.
[6] H.P.S. Shen, M.A. Oehlschlaeger, The autoignition of C8H10 aromatics at moderate temperatures and elevated pressures, Combust. Flame 156 (2009) 1053–1062.
[7] K. Seshadri, Autoignition and Combustion of Diesel and JP-8, DTIC, 2007.
[8] D. Zheng, W. Yu, B. Zhong, RP-3 aviation kerosene surrogate fuel and the chemical reaction kinetic model, Acta Phys. Chim. Sin. 31 (2015) 636–642.
[9] A. Li, Z. Zhang, X. Cheng, X. Lu, L. Zhu, Z. Huang, Development and validation of surrogates for RP-3 jet fuel based on chemical deconstruction methodology, Fuel (2020) 267.
[10] F. Battin-Leclerc, R. Bounaceur, N. Belmekki, P.A. Glaude, Experimental and modeling study of the oxidation of xylenes, Int. J. Chem. Kinet. 38 (2006) 284–302.
[11] L. Dupont, H.Q. Do, G. Capriolo, A.A. Konnov, A.El Bakali, Experimental and kinetic modeling study of para-xylene chemistry in laminar premixed flames, Fuel 239 (2019) 814–829.
[12] C.F. Goldsmith, W.H. Green, S.J. Klippenstein, Role of O_2 + QOOH in low-temperature ignition of propane.1. Temperature and pressure dependent rate coefficients, J. Phys. Chem. A 116 (2012) 3325–3346.
[13] C.K. Westbrook, M. Sjoberg, N.P. Cernansky, A new chemical kinetic method of determining RON and MON values for single component and multicomponent mixtures of engine fuels, Combust. Flame 195 (2018) 50–62.
[14] J. Zádor, C.A. Taatjes, R.X. Fernandes, Kinetics of elementary reactions in low-temperature autoignition chemistry, Prog. Energy Combust. Sci. 37 (2011) 371–421.
[15] L. Ye, L. Zhang, F. Qi, Ab initio kinetics on low temperature oxidation of iso-pentane: the first oxygen addition, Combust. Flame 190 (2018) 119–132.
[16] A. Roubaud, R. Minetti, L.R. Sochet, Oxidation and combustion of low alkylbenzenes at high pressure: comparative reactivity and auto-ignition, Combust. Flame 121 (2000) 535–541.
[17] A. Roubaud, O. Lemaire, R. Minetti, L.R. Sochet, High pressure auto-ignition and oxidation mechanisms of o-xylene, o-ethyltoluene, and n-butylbenzene between 600 and 900K, Combust. Flame 123 (2000) 561–571.
[18] X. Hui, A.K. Das, K. Kumar, C.-J. Sung, S. Dooley, F.L. Dryer, Laminar flame speeds and extinction stretch rates of selected aromatic hydrocarbons, Fuel 97 (2012) 695–702.
[19] C. Ji, E. Dames, H. Wang, F.N. Egolfopoulos, Propagation and extinction of benzene and alkylated benzene flames, Combust. Flame 159 (2012) 1070–1081.
[20] S. Gail, P. Dagaut, Experimental kinetic study of the oxidation of p-xylene in a JSR and comprehensive detailed chemical kinetic modeling, Combust. Flame 141 (2005) 281–297.
[21] S. Gail, P. Dagaut, Oxidation of m-xylene in a JSR: experimental study and detailed chemical kinetic modeling, Combust. Sci. Technol. 179 (2007) 813–844.
[22] S. Gaïl, P. Dagaut, G. Black, J.M. Simmie, Kinetics of 1,2-dimethylbenzene oxidation and ignition: experimental and detailed chemical kinetic modeling, Combust. Sci. Technol. 180 (2008) 1748–1771.
[23] B. Li, G. Liu, W. Gao, H. Cong, M. Bi, L. Ma, J. Deng, C.-.M. Shu, Study of combustion behaviour and kinetics modelling of Chinese Gongwusu coal Gangue: model-fitting and model-free approaches, Fuel 268 (2020) 117284.
[24] H.-P.S. Shen, M.A. Oehlschlarger, The autoignition of C8H10 aromatics at moderate temperatures and elevated pressures, Combust. Flame 156 (2009) 1053–1062.
[25] G. da Silva, J.W. Bozzelli, On the reactivity of methylbenzenes, Combust. Flame 157 (2010) 2175–2183.
[26] L.A. Curtiss, P.C. Redfern, K. Raghavachari, Gaussian-4 theory, J. Chem. Phys. 126 (2007) 084108.
[27] J.A. Montgomery Jr, M.J. Frisch, J.W. Ochterski, G.A. Petersson, A complete basis set model chemistry. VI. Use of density functional geometries and frequencies, J. Chem. Phys. 110 (1999) 2822–2827.
[28] K. Fukui, The path of chemical-reactions - The IRC approach, Acc. Chem. Res. 14 (1981) 363–368.
[29] M.J. Frisch, G.W. Trucks, H.B. Schlegel, G.E. Scuseria, M.A. Robb, J.R. Cheeseman, G. Scalmani, V. Barone, B. Mennucci, G.A. Petersson, H. Nakatsuji, M. Caricato, X. Li, H.P. Hratchian, A.F. Izmaylov, J. Bloino, G. Zheng, J.L. Sonnenberg, M. Hada, M. Ehara, K. Toyota, R. Fukuda, J. Hasegawa, M. Ishida, T. Nakajima, Y. Honda, O. Kitao, H. Nakai, T. Vreven, J.A. Montgomery Jr., J.E. Peralta, F. Ogliaro, M. Bearpark, J.J. Heyd, E. Brothers, K.N. Kudin, V.N. Staroverov, T. Keith, R. Kobayashi, J. Normand, K. Raghavachari, A. Rendell, J.C. Burant, S.S. Iyengar, J. Tomasi, M. Cossi, N. Rega, J.M. Millam, M. Klene, J.E. Knox, J.B. Cross, V. Bakken, C. Adamo, J. Jaramillo, R. Gomperts, R.E. Stratmann, O. Yazyev, A.J. Austin, R. Cammi, C. Pomelli, J.W. Ochterski, R.L. Martin, K. Morokuma, V.G. Zakrzewski, G.A. Voth, P. Salvador, J.J. Dannenberg, S. Dapprich, A.D. Daniels, O. Farkas, J.B. Foresman, J.V. Ortiz, J. Cioslowski, D.J. Fox, Gaussian 09, 2013 Wallingford CT.
[30] Y. Georgievskii, J.A. Miller, M.P. Burke, S.J. Klippenstein, Reformulation and solution of the master equation for multiple-well chemical reactions, J. Phys. Chem. A 117 (2013) 12146–12154.
[31] C. Eckart, The penetration of a potential barrier by electrons, Phys. Rev. 35 (1930) 1303–1309.
[32] B.E. Poling, J.M. Prausnitz, J.P. O' Connell, The Properties of Gases and Liquids, 5th ed., McGraw-Hill, Inc, New York, 2001.
[33] A.W. Jasper, C.M. Oana, J.A. Miller, Third-body" collision efficiencies for combustion modeling: hydrocarbons in atomic and diatomic baths, Proc. Combust. Inst. 35 (2015) 197–204.
[34] A. Halkier, T. Helgaker, P. Jorgensen, W. Klopper, H. Koch, J. Olsen, A.K. Wilson, Basis-set convergence in correlated calculations on Ne, N-2, and H_2O, Chem. Phys. Lett. 286 (1998) 243–252.
[35] J.A. Miller, S.J. Klippenstein, S.H. Robertson, A theoretical analysis of the reaction between ethyl and molecular oxygen, Proc. Combust. Inst. 28 (2000) 1479–1486.
[36] J.C. Rienstra-Kiracofe, W.D. Allen, H.F. Schaefer III, The C_2H_5 + O_2 reaction mechanism: high-level ab initio characterizations, J. Phys. Chem. A 104 (2000) 9823–9840.
[37] J.J. Wilke, W.D. Allen, H.F. Schaefer III, Establishment of the C_2H_5+O_2 reaction mechanism: a combustion archetype, J. Chem. Phys. 128 (2008) 074308.

[38] J.D. DeSain, C.A. Taatjes, J.A. Miller, S.J. Klippenstein, D.K. Hahn, Infrared frequency-modulation probing of product formation in alkyl + O_2 reactions: part IV. Reactions of propyl and butyl radicals with O_2, Faraday Discuss. 119 (2001) 101–120.
[39] J.D. DeSain, S.J. Klippenstein, J.A. Miller, C.A. Taatjes, Measurements, theory, and modeling of OH formation in Ethyl + O_2 and Propyl + O_2 reactions, J. Phys. Chem. A 107 (2003) 4415–4427.
[40] E.G. Estupinan, S.J. Klippenstein, C.A. Taatjes, Measurements and modeling of HO_2 formation in the reactions of n-C_3H_7 and i-C_3H_7 radicals with O_2, J. Phys. Chem. B 109 (2005) 8374–8387.
[41] H. Huang, D.J. Merthe, J. Zádor, L.E. Jusinski, C.A. Taatjes, New experiments and validated master-equation modeling for OH production in propyl + O_2 reactions, Proc. Combust. Inst. 33 (2011) 293–299.
[42] L.K. Huynh, H.H. Carstensen, A.M. Dean, Detailed modeling of low-temperature propane oxidation: 1. The role of the Propyl + O_2 reaction, J. Phys. Chem. A 114 (2010) 6594–6607.
[43] S. Canneaux, F. Louis, M. Ribaucour, A.E. Bakali, J.-F. Pauwels, A CASPT2 theoretical study of the kinetics of the 2-, 3-, and 4-methylbenzylperoxy radical isomerization, J. Phys. Chem. A 113 (2009) 2995–3003.
[44] S.M. Villano, L.K. Huynh, H.H. Carstensen, A.M. Dean, High-pressure rate rules for alkyl+ O_2 reactions. 1. The dissociation, concerted elimination, and isomerization channels of the alkyl peroxy radical, J. Phys. Chem. A 115 (2011) 13425–13442.
[45] F. Zhang, A. Nicolle, L. Xing, S.J. Klippenstein, Recombination of aromatic radicals with molecular oxygen, Proc. Combust. Inst. 36 (2017) 169–177.